X-RAYS FROM THE EXPLOSION SITE: 15 YEARS OF LIGHT CURVES OF SN 1993J

POONAM CHANDRA[1,6], VIKRAM V. DWARKADAS[2], ALAK RAY[3], STEFAN IMMLER[4], AND DAVID POOLEY[5]

[1] Department of Astronomy, University of Virginia, P.O. Box 400325, Charlottesville, VA 22904, USA; pc8s@virginia.edu
[2] Department of Astronomy and Astrophysics, University of Chicago, 5640 S Ellis Ave, AAC 010c, Chicago, IL 60637, USA
[3] Tata Institute of Fundamental Research, Mumbai 400 005, India
[4] NASA Goddard Space Flight Center, Greenbelt, MD 20771, USA
[5] University of Wisconsin, 4512 Sterling Hall, Madison, WI 53706, USA

ABSTRACT

We present a comprehensive analysis of the X-ray light curves of supernova (SN) 1993J in a nearby galaxy M81. This is the only SN other than SN 1987A, which is so extensively followed in the X-ray bands. Here, we report on SN 1993J observations with *Chandra* in the year 2005 and 2008, and *Swift* observations in 2005, 2006, and 2008. We combined these observations with all available archival data of SN 1993J, which includes *ROSAT*, *ASCA*, *Chandra*, and *XMM-Newton* observations from 1993 April to 2006 August. In this paper, we report the X-ray light curves of SN 1993J, extending up to 15 years, in the soft (0.3–2.4 keV), hard (2–8 keV), and combined (0.3–8 keV) bands. The hard- and soft-band fluxes decline at different rates initially, but after about 5 years they both undergo a t^{-1} decline. The soft X-rays, which are initially low, start dominating after a few hundred days. We interpret that most of the emission below 8 keV is coming from the reverse shock which is radiative initially for around first 1000–2000 days and then turn into adiabatic shock. Our hydrodynamic simulation also confirms the reverse shock origin of the observed light curves. We also compare the Hα line luminosity of SN 1993J with its X-ray light curve and note that the Hα line luminosity has a fairly high fraction of the X-ray emission, indicating presence of clumps in the emitting plasma.

Key words: radiation mechanisms: thermal – shock waves – supernovae: individual (SN 1993J) – X-rays: stars

Online-only material: color figures

1. INTRODUCTION

The explosion of a massive star as a supernova (SN) can drive powerful shocks into the circumstellar medium (CSM) of the progenitor. The CSM is established by the mass lost from the progenitor prior to explosion. Collision of the ejected material with the CSM leads to a blast wave shock with velocities 10,000–20,000 km s^{-1} and a hot shell of $T \sim 10^9$ K. The interface of the expanding ejecta where it first meets the CS gas is the contact discontinuity which itself propagates outward with time. As the ejecta expand, the interface region between the blast wave shock and the contact discontinuity sweeps up matter from the CS gas and decelerates due to the accumulated mass. This in turn gives rise to a shocked shell that propagates back into the cold expanding ejecta. This "reverse" shock propagates inward at $\sim 10^3$ km s^{-1}, significantly slower speed than the fastest *expanding* stellar ejecta and has a temperature of $T \sim 10^7$ K. The reverse shock is believed to be the site of most of the observable X-ray emission at late times.

In this paper, we describe the long-term light curves of the SN 1993J in various X-ray bands. We briefly describe in Section 2 the current understanding about the unusual nature of SN 1993J and its progenitor star as obtained from multi-waveband observations and theoretical analysis. We discuss the X-ray emission mechanisms and the previous X-ray studies of SN 1993J in Section 3. In Section 4, we discuss the X-ray observations and analysis of SN 1993J over the years made with several X-ray telescopes. Our detailed results and interpretation are mentioned in Section 5. Hydrodynamical simulations are discussed in Section 6, and X-ray versus optical Hα correlation in Section 7. We report our main conclusions in Section 8.

2. A SUPERNOVA THAT UNDERWENT A METAMORPHOSIS OF SPECTRAL TYPES

SN 1993J is one of the best studied SNe in all wavelength regimes, second only to SN 1987A. It was visually discovered on 1993 March 28.906 UT (Ripero & Garcia 1993), in the nearby galaxy M81 (aka NGC 3031 at $d = 3.6$ Mpc; Freedman et al. 1994). It was the optically brightest SN in the northern hemisphere since SN 1954A, having reached a secondary maximum brightness of $V = 10.8$ mag on day 21.1.

SN 1993J is a SN that has undergone an "identity crisis." Its spectrum underwent a transition from a type II spectrum (characterized by strong hydrogen Balmer lines) at early epochs, to a type Ib-like spectrum at $\approx$300 days (with its nebular spectra having weak hydrogen but strong He I lines). This SN was classified as Type IIb SN and provided for the first time a link between type II SNe and type Ib SNe (Filippenko et al. 1993; Swartz et al. 2003). Models of SN 1993J based on the early light curve indicated that the progenitor star lost all but a small amount of its hydrogen layers due to mass transfer in a binary system (Nomoto et al. 1993; Ray et al. 1993; Podsiadlowski et al. 1993; Woosley et al. 1994). Thus, the shock-heated photosphere could quickly recede through the small H layer into the deeper He layers during the initial expansion and cooling phase itself. Among core collapse SNe, it is thus possible to have a continuum of hydrogen envelope masses remaining on the progenitor star when it explodes.

At early epochs SN 1993J showed the typical signatures of CS interaction in the radio (Van Dyk et al. 1994), UV (Fransson & Sonneborn 1994), and X-ray (Zimmermann et al. 1994) wavelengths. The UV and optical spectra taken with the *Hubble Space Telescope* (*HST*) and Keck telescopes have revealed the signature of a massive star, along with the fading SN 10 years

---

[6] Jansky Fellow, National Radio Astronomy Observatory

after explosion, which is the binary companion of the progenitor that exploded (Maund et al. 2004). The CSM has therefore been modified by the mass loss in a binary system in SN 1993J.

3. X-RAY EMISSION AND EARLY X-RAY STUDIES OF SN 1993J

The X-ray luminosity and its time variation depend, among other things, on the density structure of the stellar ejecta. In core collapse SNe, the explosion dynamics quickly lead to an ejecta outer density profile with a steep power law ($\rho_{ej} \propto r^{-n}$, where n is a constant) in the radial coordinate, but with a relatively flat inner core density profile (Chevalier and Soker 1989; Matzner & McKee 1999). The ejecta density profile depends on the initial structure of the star and, in particular, is affected by if the progenitor had a radiative or a convective envelope (Matzner & McKee 1999). The shock propagation through the outer profile does not depend upon the behavior of the inner layers and a limiting structure is described by a self-similar solution as the shock front accelerates while propagating through the outer layers with rapidly decreasing density. The self-similar nature of the evolution of the ejecta-dominated SNe (or supernova remnants (SNRs)) applies only for ejecta with steep envelope index $n > 5$, since for such steep n, the mass and energy of the ejecta remain finite (Truelove & McKee 1999).

The shocked shells (forward or reverse) generated due to ejecta-wind interaction have very high temperatures (Section 1) and can emit X-rays. The forward shock is adiabatic almost all the time and its luminosity follows the time dependence of $L_{forward} \propto t^{-1}$ (Chevalier & Fransson 2003). However, depending upon the ejecta density profile and the mass-loss rate of the SN progenitor star, the reverse shock can either be adiabatic or radiative, or can be radiative at early phase and then make a transition to adiabatic phase. The expression for free–free emission from adiabatic reverse shock and its luminosity is derived by Chevalier & Fransson (2003) and Fransson et al. (1996):

$$L_{rev}^{ad} \approx 3 \times 10^{40} \bar{g}_{ff} \frac{(n-3)(n-4)^2}{4(n-2)} \left(\frac{\dot{M}_{-5}}{u_{w1}}\right)^2 \left(\frac{t}{1\,\text{day}}\right)^{-1} \text{erg s}^{-1}. \tag{1}$$

Here $\dot{M}_{-5}$ is progenitor mass-loss rate in units of $10^{-5}\,M_\odot\,\text{yr}^{-1}$, u_{w1} is the wind velocity in units of $10\,\text{km s}^{-1}$, and $\bar{g}_{ff}$ is the free–free Gaunt factor. This shows that free–free emission from adiabatic reverse shock follows time evolution of t^{-1} for constant mass-loss rate and wind velocity. However, if line emission dominates, the time dependence of X-ray line luminosity is $t^{1.2-2.2m}$ (Chevalier & Fransson 1994), where m is the expansion parameter in $R \propto t^m$.

Fransson et al. (1996) have discussed that in the initial phase, reverse shock with high density gradient is likely to be radiative resulting in formation of a cooled shell between the reverse shock and the forward shock. When the electron temperature is $T_e \leqslant 2 \times 10^7$ K, the line emission dominates the total X-ray emission. Chevalier & Fransson (2003) have discussed the importance of line emission and its effect on the cooling rate of the gas behind the reverse shock. In case of line emission, a thermal instability develops and the gas cools up to about 10^4 K where the temperature is stabilized only by photoelectric heating from the shock balancing the cooling. For an ejecta velocity scale of V_{ej}, and a reverse shock moving through an ejecta density gradient $\rho \propto r^{-n}$ with solar composition one obtains a cooling timescale from $t_{cool} = 3kT_e/n\Lambda$, where Λ

is the cooling function. The cooling time can be expanded as (Fransson et al. 1996; Chevalier & Fransson 2003)

$$t_{cool} = \frac{605}{(n-3)(n-4)(n-2)^{3.34}} \left(\frac{V_{ej}}{10^4\,\text{km s}^{-1}}\right)^{5.34}$$
$$\times \left(\frac{\dot{M}_{-5}}{u_{w1}}\right)^{-1} \left(\frac{t}{1\,\text{day}}\right)^2 \text{days.} \tag{2}$$

Since large exponents of the velocity scale and density gradient index are involved, it is clear that the cooling time is sensitive to them, and also the mass-loss rate of the pre-explosion progenitor star. The most important effect of cooling gas between the reverse shock and the observer is that the cool gas absorbs most of the emission from the reverse shock, and in spite of the higher intrinsic luminosity of the reverse shock, little of it will be directly observable initially. The column density of the cool gas also thins out as the SN ages and expands in scale. In such a situation the total luminosity of the reverse shock may contribute appreciably, or even dominate, to the bolometric luminosity and is defined as

$$L_{rev}^{rad} = 1.6 \times 10^{41} \frac{(n-3)(n-4)}{(n-2)^3} \left(\frac{\dot{M}_{-5}}{u_{w1}}\right)$$
$$\times \left(\frac{V_{rev}}{10^4\,\text{km s}^{-1}}\right)^3 \text{erg s}^{-1}. \tag{3}$$

Since $V_{rev} \propto t^{-1/(n-2)}$, the time dependence of luminosity in cooling case is $L_{rev}^{rad} \propto t^{-3/(n-2)}$. In Table 3, we tabulate the timescales up to which the reverse shock remains radiative under different conditions. We take the case with density index of 7, 12, and, 20 for three compositions: solar, helium, and oxygen. As one can see from the table, the deeper in the ejecta the reverse shock (where the composition is dominated by heavier elements) is, the longer time do the reverse shocks remain radiative.

It has been argued that SN 1993J-like objects with their high mass-loss rate will have radiative reverse shocks (where cooling is important) even at late epochs ($\geqslant 100$ days) whereas SNe with low mass-loss rates such as SN 1999em (a type IIP SN) with long cooling times will develop adiabatic reverse shocks early on (Nymark et al. 2006). However, in some cases adiabatic and radiative reverse shocks co-exist as has been seen in SN 1987A (Gröningsson et al. 2006). Nymark et al. (2009) has discussed that if the ejecta or the CSM is clumpy, the adiabatic reverse shock may give rise to slow moving oblique shocks which are radiative in nature.

Soon after its discovery SN 1993J was observed and detected in the X-rays by *ROSAT* (Zimmermann et al. 1993). Since then, the SN has been observed at various epochs with a number of X-ray telescopes, including *ROSAT* (Zimmermann et al. 1994; Immler et al. 2001), *ASCA* (Tanaka 1993; Kohmura et al. 1994; Uno et al. 2002), *Chandra* (Swartz et al. 2003, and this paper), *XMM-Newton* (Zimmermann & Aschenbach 2003), and *Swift* (this paper) satellite missions. The Oriented Scintillation Spectrometer Experiment (OSSE) on the *Compton Observatory* had detected the SN in 50–150 keV energy band on day 12 and 30 with very high X-ray luminosity (5×10^{40} erg s^{-1}) on day 12 (Leising et al. 1994). However, they found that the 50–150 keV emission faded below detection by day 108.

Suzuki et al. (1993) did a detailed analysis of the early X-ray emission from the SN. They carried out hydrodynamical modeling of the collision between the ejecta and a CSM created by steady winds ($\rho_{CSM} \propto r^{-2}$), and claimed that the observed

CHANDRA ET AL.

Table 1
Details of X-ray Observations of SN 1993J

Date of Observation	Mission	Instrument	Observation ID	Exposure (ks)
1993 Apr 03.41	*ROSAT*	PSPC	RP180015N00	. . .
1993 Apr 05.25–Apr 06.04	*ASCA*	. . .	15000120	27.4
1993 Apr 07.25–Apr 07.94	*ASCA*	. . .	15000130	28.3
1993 Apr 08.34–Apr 09.35	*ROSAT*	PSPC	RP180015N00	. . .
1993 Apr 12.23–Apr 13.01	*ROSAT*	PSPC	RP180015N00	. . .
1993 Apr 16.83	*ROSAT*	PSPC	RP180015N00	5.1
1993 Apr 16.94–Apr 18.73	*ASCA*	. . .	15000030	66.4
1993 Apr 17.68–Apr 19.68	*ROSAT*	HRI	RH600247A01	. . .
1993 Apr 22.05–Apr 24.0	*ROSAT*	PSPC	RP180015N00	. . .
1993 Apr 25.76	*ASCA*	. . .	15000020	11.1
1993 May 01.93–May 02.59	*ASCA*	. . .	15000040	21.6
1993 May 04.30–May 06.30	*ROSAT*	PSPC	RP180015A01	. . .
1993 May 12.85–May 13.48	*ROSAT*	HRI	RH600247	. . .
1993 May 18.87–May 19.86	*ASCA*	. . .	15000050	39.3
1993 Oct 24.60–Oct 25.59	*ASCA*	. . .	10018000	39.6
1993 Nov 01.68	*ROSAT*	PSPC	RP180035N00	. . .
1993 Nov 07.90	*ROSAT*	PSPC	RP180035A01	20.0
1994 Apr 01.45	*ROSAT*	PSPC	RP180050N00	108.3
1994 Apr 01.68	*ASCA*	. . .	51005000	32.6
1994 Oct 19.17–Oct 21.31	*ROSAT*	HRI	RH600739N00	. . .
1994 Oct 21.18–Oct 22.33	*ASCA*	. . .	52009000	46.4
1995 Apr 13.71–May 04.90	*ROSAT*	HRI	RH600740N00	. . .
1995 Oct 19.00	*ROSAT*	HRI	RH600881N00	. . .
1996 Apr 15.88–May 07.83	*ROSAT*	HRI	RH600882N00	. . .
1996 Nov 04.50	*ROSAT*	HRI	RH600882A01	. . .
1997 Mar 31.10	*ROSAT*	HRI	RH601001N00	. . .
1997 Sep 30.44–Oct 16.00	*ROSAT*	HRI	RH601002N00	. . .
1998 Mar 26.10	*ROSAT*	HRI	RH601095N00	. . .
2000 Mar 21.03	*Chandra*	ACIS-S (NONE)	390	2.4
2000 May 07.23	*Chandra*	ACIS-S (NONE)	735	50.6
2001 Apr 22.32	*XMM-Newton*	EPIC-PN	0111800301	132.0
2005 Aug 14.41	*Chandra*	ACIS-S (HETG)	5600	36.4
2005 Jul 19.60	*Chandra*	ACIS-S (HETG)	5601	84.1
2005 Jul 14.81	*Chandra*	ACIS-S (HETG)	6347	64.7
2005 Jul 14.07	*Chandra*	ACIS-S (HETG)	6346	55.2
2005 Feb 24.29	*Chandra*	ACIS-S (HETG)	6174	45.2
2006 Jul 13.57	*Chandra*	ACIS-S (HETG)	6899	15.1
2006 Feb 08.85	*Chandra*	ACIS-S (HETG)	6892	15.0
2006 Mar 05.99	*Chandra*	ACIS-S (HETG)	6893	15.0
2006 Apr 01.44	*Chandra*	ACIS-S (HETG)	6894	15.0
2006 May 14.54	*Chandra*	ACIS-S (HETG)	6896	15.0
2006 Jun 09.76	*Chandra*	ACIS-S (HETG)	6897	15.0
2006 Aug 12.68	*Chandra*	ACIS-S (HETG)	6901	15.0
2006 Jun 28.98	*Chandra*	ACIS-S (HETG)	6898	14.9
2006 Apr 24.35	*Chandra*	ACIS-S (HETG)	6895	14.7
2006 Jul 28.46	*Chandra*	ACIS-S (HETG)	6900	14.6
2005 Jul 03.06	*Chandra*	ACIS-S (NONE)	5948	12.2
2005 Jul 06.33	*Chandra*	ACIS-S (NONE)	5949	12.2
2005 Jun 18.48	*Chandra*	ACIS-S (NONE)	5943	12.2
2005 Jun 26.90	*Chandra*	ACIS-S (NONE)	5946	12.2
2005 Jun 01.36	*Chandra*	ACIS-S (NONE)	5937	12.2
2005 Jun 09.29	*Chandra*	ACIS-S (NONE)	5940	12.1
2005 Jun 15.06	*Chandra*	ACIS-S (NONE)	5942	12.1
2005 Jun 03.95	*Chandra*	ACIS-S (NONE)	5938	12.0
2005 Jun 06.64	*Chandra*	ACIS-S (NONE)	5939	12.0
2005 Jun 11.89	*Chandra*	ACIS-S (NONE)	5941	12.0
2005 Jun 21.22	*Chandra*	ACIS-S (NONE)	5944	12.0
2005 Jun 24.25	*Chandra*	ACIS-S (NONE)	5945	11.7
2005 May 28.83	*Chandra*	ACIS-S (NONE)	5936	11.6
2005 May 26.16	*Chandra*	ACIS-S (NONE)	5935	11.1
2005 Jun 29.56	*Chandra*	ACIS-S (NONE)	5947	10.8
2005 Apr 21.00	*Swift*	XRT	00035059001	1.6
2005 Aug 25.05	*Swift*	XRT	00035059002	5.1
2006 Jun 24.00	*Swift*	XRT	00035059003	4.2

Table 1
(Continued)

Date of Observation	Mission	Instrument	Observation ID	Exposure (ks)
2006 Nov 18.04	*Swift*	XRT	00035059004	21.2
2008 Jan 09.04	*Swift*	XRT	00036557001	4.4
2008 Jan 11.59	*Swift*	XRT	00036557002	3.6
2008 Jan 15.47	*Swift*	XRT	00036557003	1.4
2008 Feb 01.00	*Chandra*	ACIS-S (NONE)	9122	10.0

Table 2
Unabsorbed X-ray Luminosities of SN 1993J at Various Epochs

Date of Observation	Days Since Explosion	Instrument	Luminosity (10^{38} erg) 0.3–2.4 keV	2–8 keV	0.3–8 keV
1993 Apr 03.41	6.61	*ROSAT*-PSPC	20.63 ± 1.20	. . .	. . .
1993 Apr 05.25–Apr 06.04	8.45–9.24	*ASCA*	20.50 ± 5.99	133.02 ± 20.27	166.85 ± 21.29
1993 Apr 07.25–Apr 07.94	10.45–11.14	*ASCA*	19.71 ± 3.00	127.48 ± 13.31	156.91 ± 10.72
1993 Apr 08.34–Apr 09.35	11.54–12.55	*ROSAT*-PSPC	18.76 ± 0.92	. . .	. . .
1993 Apr 12.23–Apr 13.01	15.43–16.24	*ROSAT*-PSPC	15.63 ± 0.76	. . .	. . .
1993 Apr 16.83	20.03	*ROSAT*-PSPC	14.96 ± 2.52	. . .	. . .
1993 Apr 16.94–Apr 18.73	20.14-21.93	*ASCA*	13.56 ± 3.15	69.27 ± 8.32	87.37 ± 5.36
1993 Apr 17.68–Apr 19.68	20.88–22.88	*ROSAT*-HRI	16.54 ± 0.96	. . .	. . .
1993 Apr 22.05–Apr 24.0	25.25–27.20	*ROSAT*-PSPC	14.20 ± 0.63	. . .	. . .
1993 Apr 25.76	28.96	*ASCA*	. . .	52.91 ± 11.62	78.22 ± 10.72
1993 May 01.93–May 02.59	35.13–35.79	*ASCA*	14.82 ± 8.52	51.43 ± 8.68	67.97 ± 14.51
1993 May 04.30–May 06.30	37.50–39.50	*ROSAT*-PSPC	13.66 ± 0.54	. . .	. . .
1993 May 12.85–May 13.48	46.05–46.68	*ROSAT*-HRI	12.47 ± 1.07	. . .	. . .
1993 May 18.87–May 19.86	52.07–53.06	*ASCA*	13.88 ± 6.15	29.16 ± 3.97	50.15 ± 14.04
1993 Oct 24.60–Oct 25.59	203.30–204.29	*ASCA*	. . .	3.84 ± 2.74	. . .
1993 Nov 01.68	211.38	*ROSAT*-PSPC	7.47 ± 0.23	. . .	. . .
1993 Nov 07.90	217.60	*ROSAT*-PSPC	8.08 ± 0.50	. . .	. . .
1994 Apr 01.45	362.15	*ROSAT*-PSPC	3.59 ± 0.52	. . .	. . .
1994 Apr 01.68	362.38	*ASCA*	8.83 ± 3.15	2.30 ± 2.06	11.51 ± 5.36
1994 Oct 19.17–Oct 21.31	562.82–564.96	*ROSAT*-HRI	4.35 ± 0.36	. . .	. . .
1994 Oct 21.18–Oct 22.33	564.83–565.98	*ASCA*	4.89 ± 2.37	<0.47	4.89 ± 1.89
1995 Apr 13.71–May 04.90	739.36–763.70	*ROSAT*-HRI	5.35 ± 0.43	. . .	. . .
1995 Oct 19.00	909.65	*ROSAT*-HRI	6.74 ± 0.48	. . .	. . .
1996 Apr 15.88–May 07.83	1106.53–1144.48	*ROSAT*-HRI	6.59 ± 0.48	. . .	. . .
1996 Nov 04.50	1309.15	*ROSAT*-HRI	5.54 ± 0.80	. . .	. . .
1997 Mar 31.10	1455.75	*ROSAT*-HRI	6.26 ± 0.46	. . .	. . .
1997 Sep 30.44–Oct 16.00	1639.09–1654.65	*ROSAT*-HRI	5.83 ± 0.43	. . .	. . .
1998 Mar 26.10	1815.75	*ROSAT*-HRI	4.08 ± 0.50	. . .	. . .
2000 Mar 21.03	2541.68	*Chandra* ACIS-S	4.44 ± 1.40	1.75 ± 0.44	5.89 ± 1.69
2000 May 07.23	2588.88	*Chandra* ACIS-S	3.88 ± 0.14	1.66 ± 0.18	5.26 ± 0.40
2001 Apr 22.32	2938.97	*XMM-Newton* EPIC-PN	4.54 ± 0.25	1.25 ± 0.24	5.55 ± 0.44
2005 Feb 24.29–Aug 14.41[a]	4341.94–4513.06	*Chandra* ACIS-S (HETG)	1.77 ± 0.18	0.43 ± 0.08	2.10 ± 0.20
2005 Apr 21.00–Aug 25.05[b]	4397.65–4523.70	*Swift*-XRT	<2.24	<0.41	<2.46
2005 May 26.16–Jun 15.07[c]	4432.81–4452.72	*Chandra* ACIS-S	2.16 ± 0.11	0.46 ± 0.02	2.53 ± 0.13
2005 Jun 18.48–Jul 06.33[d]	4456.13–4473.98	*Chandra* ACIS-S	2.24 ± 0.38	0.49 ± 0.10	2.63 ± 0.44
2006 Feb 08.85–Aug 12.68[e]	4691.5–4876.33	*Chandra* ACIS-S(HETG)	1.61 ± 0.60	0.24 ± 0.07	1.78 ± 0.67
2006 Jun 24.00–Nov 18.04[f]	4826.65-4973.69	*Swift*-XRT	1.91 ± 0.32	0.33 ± 0.05	2.08 ± 0.35
2008 Jan 09.04–15.47[g]	5385.69-5392.12	*Swift*-XRT	2.02 ± 0.55	0.37 ± 0.08	2.22 ± 0.59
2008 Feb 01.00	5407.65	*Chandra* ACIS-S	1.67 ± 0.1	0.30 ± 0.08	1.85 ± 0.1

Notes.
[a] Combined observations with IDs 5600, 5601, 6174, 6346, and 6347.
[b] Combined observations with IDs 00035059001 and 00035059002.
[c] Combined observations with IDs 5935, 5936, 5937, 5939, 5940, and 5941.
[d] Combined observations with IDs 5943, 5944, 5945, 5946, 5947, 5948, and 5949.
[e] Combined observations with IDs 6892–6901.
[f] Combined observations with IDs 00035059003 and 00035059004.
[g] Combined observations with IDs 00036557001, 00036557002, and 00036557003.

features of X-ray emission can be accounted for with thermal free–free emission from the shock-heated ejecta. They also predicted that the expansion velocities of the ejecta must be high and the density gradient of the ejecta shallow. Later they extended their analysis to X-ray observations of first 600 days in Suzuki & Nomoto (1995). In this paper, they assumed a more

Table 3
Timescales in Days for Reverse Shock to Remain Radiative for Various Values of Ejecta Velocity, Mass-loss Rate, Composition and Density Index[a]

Composition	Density Index (n)	$V_4 = 0.5$			$V_4 = 1.0$			$V_4 = 2.0$		
		$\dot{M}_{-5} = 1$	$\dot{M}_{-5} = 4$	$\dot{M}_{-5} = 10$	$\dot{M}_{-5} = 1$	$\dot{M}_{-5} = 4$	$\dot{M}_{-5} = 10$	$\dot{M}_{-5} = 1$	$\dot{M}_{-5} = 4$	$\dot{M}_{-5} = 10$
Solar	7	60	250	570	4	16	40	0.4	1.6	4
	12	3080	1.2×10^4	3×10^5	160	630	1580	8	32	80
	20	1.3×10^5	5.2×10^5	1.3×10^6	3000	1.2×10^4	2.9×10^4	125	500	1250
Helium	7	190	760	1900	19	76	190	2	8	20
	12	1.2×10^4	4.9×10^4	1.2×10^5	473	1900	4730	40	160	400
	20	4.4×10^5	1.8×10^6	4.4×10^6	1.2×10^4	4.9×10^4	1.2×10^5	400	1700	4000
Oxygen	7	6310	2.5×10^4	6.3×10^4	470	1900	4700	42	170	420
	12	5.5×10^5	2.2×10^6	5.5×10^6	1.7×10^4	6.6×10^4	1.7×10^5	977	3900	9770
	20	3×10^7	1.2×10^8	3×10^8	5.5×10^5	2.2×10^6	5.5×10^6	1.5×10^4	5.9×10^4	1.5×10^5

Note.

[a] In this table V_4 is the ejecta velocity in 10^4 km s^{-1}, and $\dot{M}_{-5}$ is mass-loss rate in units of $10^{-5} M_\odot$ yr^{-1}.

realistic ejecta model, a steep density gradient in the outermost layer followed by a much shallow density gradient in the inner H-rich envelope. The density profile suddenly increases and becomes steeper again at the interface of H-rich envelope and the He-core. The CSM was assumed to be clumpy and cooling effects were taken into account with the formation of a dense cooling shell between the reverse and the forward shock. Early X-rays from the reverse shock were absorbed in this cool shell and X-rays were mainly the thermal emission from the shocked CSM. Their results indicated that the CSM has density distribution of the nature $\rho_{CSM} \propto r^{-1.7}$ instead of $\rho_{CSM} \propto r^{-2}$, indicating that the CSM was created by non-steady winds. According to their model, the CSM has to be more clumpy in the outer layers to explain the observed X-ray features. The collisions between the forward shock and the clumps may give rise to soft X-rays. Such collisions would take place with many clumps at various distances, and the sum of resulting X-ray emissions may form a more or less continuous light curve. In their model, all the soft X-rays in first few tens of days were coming from the clumpy CSM, and had no contribution from the reverse shell as they were totally absorbed by the cooled shell. However, in Nomoto & Suzuki (1998), they revised their prediction and claimed that the cooling dense shell formed between the reverse and the forward shocked shell is clumpy due to the Rayleigh–Taylor instability and thus some early X-rays may also leak out from reverse shock. They also predicted the possible increase in the soft X-rays around day 500 to be due to the density jump from the H-rich envelope to He layer, modified by the Rayleigh–Taylor instabilities.

Fransson et al. (1996) have studied the early-time X-ray emission from SN 1993J in detail. Using radio and X-ray observations from the first two weeks, they estimated the mass loss rate of $\sim 4 \times 10^{-5} M_\odot \; yr^{-1}$. Fitting the early radio data using the free–free absorption model, they suggested a wind density profile: $\rho_{CSM} \propto r^{-1.5}$. They did the detailed analysis of X-ray data from *ROSAT*, *ASCA* and OSSE on the *Compton Observatory*. According to their conclusion, the early hard X-rays arise mainly from the CS shock, whereas the high column density of the cooling shell between the CS shock and the radiative reverse shock absorbs most of the soft X-ray emission arising from the radiative reverse shock. After about 50-100 days the column density of the cooling shell decreases enough for the X-rays from the reverse shock to leak out and dominate the spectrum. They also found that the X-ray observations are best fit with the flatter CSM density profile of $\rho_{CSM} \propto r^{-1.7}$. However, in their later work Fransson & Bjornsson (1998) claimed that the CSM density profile is more sensitive to the

radio observations and they found the radio observations to be fitting well in $\rho_{CSM} \propto r^{-2}$ profile. The earlier discrepancy in radio band was claimed to be due to neglecting the synchrotron-self absorption process which plays an important role in the radio absorption for SN 1993J. However, Mioduszewski et al. (2001) included both synchrotron self-absorption and free–free absorption in their analysis and claimed that the radio emission could not be fitted with a CSM declining as r^{-2}, but that a density profile going as $r^{-1.7}$ provided a much better fit. In this paper, we use the CSM profile to be $\rho_{CSM} \propto r^{-2}$, though we explore the possibility of different profiles in Section 6.

4. OBSERVATIONS AND ANALYSIS

As mentioned in Section 3, SN 1993J has been observed at various epochs with multiple X-ray telescopes since its discovery. Below, we describe these observations in detail. We analyzed the 2005 and 2008 *Chandra* data and the *Swift* data at several epochs between 2006–2008. We also reanalyzed the 2001 *XMM-Newton* and 2000 *Chandra* data sets and extracted unabsorbed fluxes in 0.3–2.4 keV, 2–8 keV, and 0.3–8 keV bands. For *ROSAT* and *ASCA*, we extracted unabsorbed fluxes in the above bands using best-fit parameters mentioned in various references (see below). In our fits, the column density is a measure of the absorbing cool shell in the SN plus the galactic absorption shell. The column density was set to zero to extract the absorption corrected luminosities. Below we describe the various SN 1993J X-ray observations in detail. The details of all observations used in this paper are summarized in Table 1.

4.1. ROSAT *Observations*

X-ray observations of SN 1993J by *ROSAT* between days 6 and 1181 after explosion were reported by Immler et al. (2001), in which both PSPC and HRI observations were included. HRI data were binned in observation blocks of length 5–20 ks exposure time whereas the PSPC observation blocks had integration times ranging 2–18 ks long. They had assumed a constant absorption column density and extracted the fluxes. Zimmermann & Aschenbach (2003) reanalyzed all the *ROSAT* data and reported the observations up to day 1800. They fitted all the spectra assuming column density as a free parameter and with a thermal-plasma model with a single temperature (vmekal in XSPEC) fixing the element abundances to that obtained from, e.g., *XMM-Newton* EPIC-PN spectrum. They found that due to the high temperatures in the early *ROSAT* observations there is almost no difference between fitting either with solar or with the *XMM-Newton* elemental abundances. We use the best-fit

parameters quoted in Table 3 of Zimmermann & Aschenbach (2003) to extract the *ROSAT* fluxes of the SN at various epochs. Table 2 shows the unabsorbed luminosities for the *ROSAT*-HRI and *ROSAT*-PSPC observations in the energy range of 0.3– 2.4 keV.

4.2. ASCA *Observations*

ASCA flux points were extracted from Kohmura et al. (1994), Uno et al. (2002), and Swartz et al. (2003). The large field of view (FoV) of *ASCA* showed the presence of the SN host galaxy and a bright X-ray binary source at respectively 3′ and 1′ away from the SN. Since *ASCA* point-spread function has a resolution of 3′, the bright X-ray binary was strongly contaminating the SN flux. To avoid this contamination Kohmura et al. (1994) and Uno et al. (2002) isolated SN 1993J flux through a one-dimensional image fitting, by using 1′ × 2′ rectangular boxes containing the SN and the X-ray binary separately, and by modeling the one-dimensional intensity profile. They claimed to get rid of almost all the contamination from the M81 and the X-ray binary source, by this method.

To estimate more reliable *ASCA* fluxes of SN 1993J, we attempted to utilize the late *Chandra* observations. Due to its high angular resolution, *Chandra* is able to easily separate the SN, and the nearby X-ray binary and M81 nucleus. Our aim was to extract the uncontaminated flux of the X-ray binary and then subtract it from all the *ASCA* observations. However, for this technique to work, we needed to make sure that the X-ray binary is not a time variable source. To determine this, we analyzed two *Chandra* data sets, one of 2000 May 7 and another on 2005 Jun 01 and extracted the flux of the X-ray binary from both the data, respectively. Our analysis shows that the X-ray binary is a highly variable source, especially in the hard X-rays. The 0.3–8.0 keV flux decreases by a factor of 2 in 5 years, from 2.79×10^{-12} erg cm^{-2} s^{-1} in 2000 May to 1.40×10^{-12} erg cm^{-2} s^{-1} in 2005 June. The change in the SN flux at 2–8 keV is by more than a factor of 3 in the two observations (2.26×10^{-12} erg cm^{-2} s^{-1} in 2000 May to 6.9×10^{-13} erg cm^{-2} s^{-1} in 2005 June). Thus, in view of high variability of the X-ray binary source, it is not advisable to reanalyze all the *ASCA* data sets to remove the contribution of the X-ray binary on the basis of *Chandra* flux of the binary. We use the spectral fit parameters of Kohmura et al. (1994) and Uno et al. (2002) to convert the count rates into unabsorbed fluxes in bands 0.3–2.4, 2–8 and 0.3–8 keV fluxes (Table 2).

4.3. Chandra *Observations*

Chandra first observed SN 1993J on 2000 March 21 and 2000 May 07 under ObsIDs 390 and 735 with ACIS-S by Swartz et al. (2003). They showed that SN 1993J faded since its discovery and its spectrum softened. At this time SN 1993J was ∼2600 days old and displayed a complex thermal spectrum from a reverse shock rich in Fe L and highly ionized Mg, Si, and S but lacking oxygen. The unabsorbed luminosity reported in Table 2 are extracted from Swartz et al. (2003).

Chandra ACIS-S observed the SN starting from 2005 May 26 to 2005 July 6, on 15 different occasions (Obs Ids: 5935-5949; PI: Pooley). Each observation was around 11–12 ks. We analyzed this data using CIAO analysis threads and XSPEC. Event 2 files (pipeline processed files) were used for the data analysis. Standard methods were used to analyze the data (Chandra et al. 2005). We combined the whole data set in two groups to increase the signal-to-noise ratio and extracted
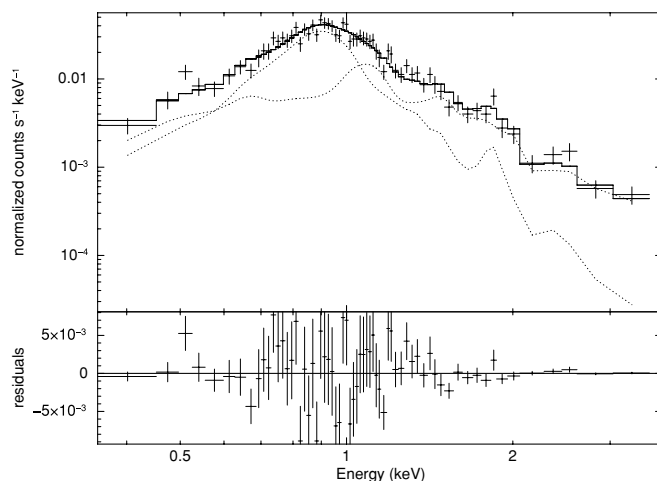
Figure 1. Here we plot the two component Mekal fit to SN 1993J *Chandra* data of 2005 taken with ACIS-S. Best-fit temperatures from the Mekal model are 0.73 keV and 2.21 keV with absorption column density of 6×10^{20} cm^{-2}.

the unabsorbed fluxes at various epochs in 0.3–2.4 and 2.0–8.0 keV ranges. We also did spectral analysis of ∼180 ks *Chandra* ACIS-S data in 2005 given its large exposure. We get an excellent fit to the data using a two-component thermal-plasma model (reduced χ^2 of 1.09) with absorption column density of $(6.0 \pm 1.5) \times 10^{20}$ cm^{-2}. This is close to the Galactic absorption in the direction of M81, which is expected at such late epochs when the cool shell absorption may have become insignificant. The two temperatures obtained from the best fit are 0.73 ± 0.04 keV and 2.21 ± 0.24 keV. Other models do not fit the data well. The non-equilibrium ionization (NEI) model gives reduced $\chi^2 = 1.88$ for 104 degrees of freedom and power-law model gives reduced $\chi^2 = 3.48$ for 105 degrees of freedom. The two-temperature bremsstrahlung model yields a reduced $\chi^2 = 1.90$ for 103 degrees of freedom. Hence, the two-component thermal-plasma model is the most plausible one. We could not fit the various lines to the data given its sparseness. We plot the spectral fit to this data in Figure 1.

We also extracted the archival data observed with *Chandra* ACIS-S in HETG mode on 15 occasions from 2005 February 24 to 2006 August 12 (Obs IDs: 6174, 6346-47, 5600-01, 6892-6901; PI: Canizares) and analyzed it. These observations were taken for M81, the host galaxy of SN 1993J which is 3′ away from the SN. SN 1993J flux was a byproduct of these observations. Half of the observations were centered on ACIS chip S2 and the rest of the half on S3. We combined all the data sets in these two major sets and extracted the flux using best-fit models. In this case, we fixed the column density to be 0.06×10^{22} cm^{-1}, the one obtained from the 2005 *Chandra* observations (see above).

Latest observations of SN 1993J with *Chandra* was taken on 2008 February 1 (PI: Immler). The observations were taken in ACIS-S mode without any grating. The total exposure time was 14.80 ks, out of which we could extract 10 ks of good data. The count rate in this observation was $(2.22 \pm 0.15) \times 10^{-2}$ counts in full ACIS band. We converted these count rate into flux using $N_H = 0.06 \times 10^{22}$ cm^{-1} and temperature of 0.7 keV.

4.4. XMM-Newton *Observations*

XMM-Newton observed SN 1993J on 2001 April 22 around 8 years after the explosion for about 132 ks duration, under obsID 0111800301 (Zimmermann & Aschenbach 2003). Data
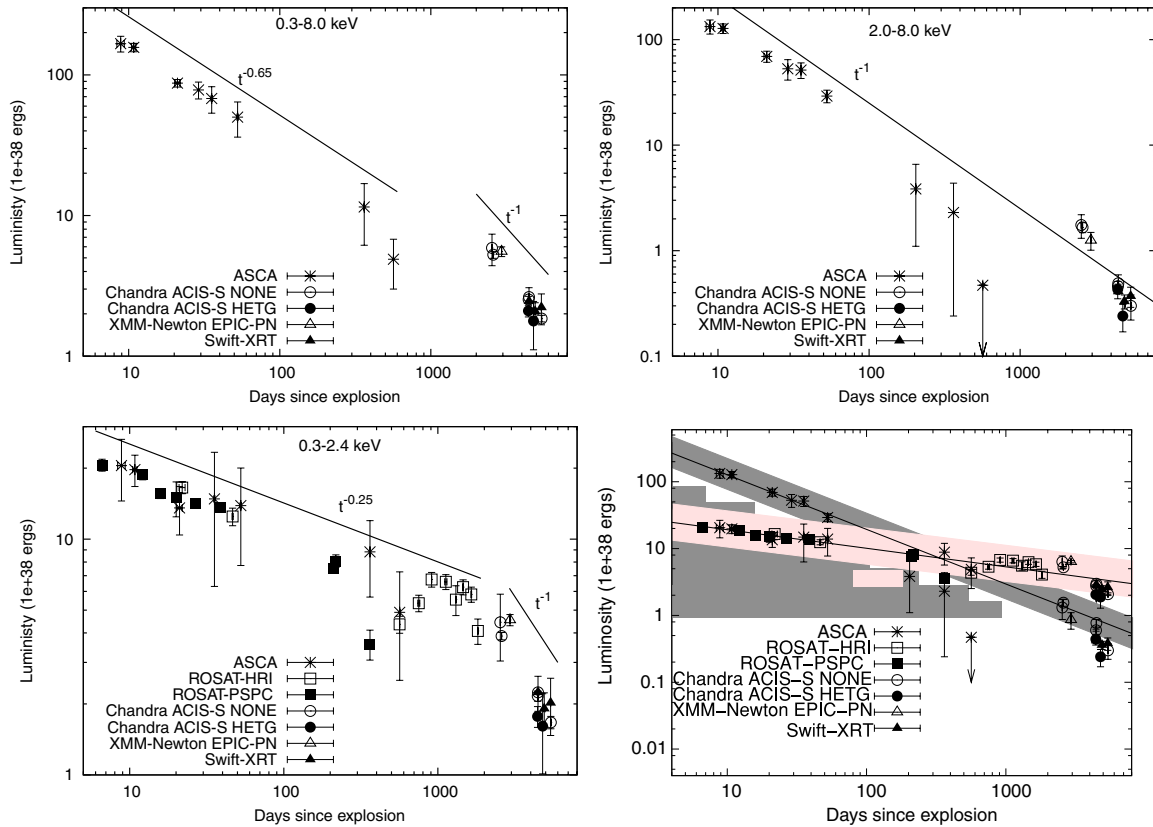
Figure 2. X-ray light curves of SN 1993J in the 0.3–8 keV (upper left panel), 2–8 keV (upper right panel), and 0.3–2.4 keV (lower left panel) bands observed with multiple telescopes. For around first 1000 days, 0.3–2.4 keV light curves declines slowly ($t^{-0.25}$) whereas the 2–8 keV light curves decline as t^{-1}. The overall 0.3–8 keV light curve declines as $t^{-0.65}$ indicating radiative nature of the reverse shock. After around day 1000, the shocks seem to become adiabatic. The lower right panel shows the comparison between the 0.3–2.4 keV and 2–8 keV components and demonstrates that the soft component takes over around day 200 and dominates at late epochs.

(A color version of this figure is available in the online journal.)

from the EPIC PN camera, run in small window mode, and the MOS2 camera in imaging mode were obtained. Zimmermann & Aschenbach ([2003](#)) did the detailed analysis of the data and fit the X-ray spectrum with two-component thermal-plasma model. They claimed emissions from highly ionized Mg, Si, S, Ar, Ca, and complex Fe. We used their best fit parameters to extract the unabsorbed luminosity in 0.3–2.4 keV, 2–8 keV and 0.3–8 keV bands.

4.5. Swift *Observations*

The X-Ray Telescope (XRT; Burrows et al. [2005](#)) on board the *Swift* Observatory (Gehrels et al. [2004](#)) observed SN 1993J on 2005 April 21, 2005 August 25, 2006 June 24, 2006 November 18–20, and on 2008 January 09–15. We combine the data closely spaced in time, i.e., 2005 April 21–August 25, 2006 June 24–November 18, and 2008 January 09–15, to increase the sensitivity of the data.

The HEASOFT[7] (version 6.2) and *Swift* software (version 2.6.1, build 20) tools and latest calibration products were used to reanalyze the data. X-ray counts were extracted from a circular region with a 10 pixel (24″) radius centered on the optical position of the SN. The background was extracted locally from a source-free region of 30″ radius and corrected for the 100% encircled energy radius, to account for the detector and the sky background, and for residual diffuse emission from the host galaxy. SN 1993J is detected in X-rays in the

21 ks XRT observation from 2006 November 18 to 20 at a 7.0σ significance of source detection and a net count rate of $(4.1 \pm 0.6) \times 10^{-3}$ counts s^{-1} (0.2–10 keV). Table [2](#) gives details of these observations.

5. RESULTS AND INTERPRETATION

We tabulate the details of all the above observations described in Section [4](#) in Table [1](#). We report the unabsorbed luminosities in 0.3–2.4, 2–8 and 0.3–8 keV bands in Table [2](#). We plot the light curves constructed in these bands from the above observations in Figure [2](#). The light curve in 0.3–8 keV shows linear decline with power-law index of −0.65 for first few hundred days. At late epochs, from day 2500 onward, the light curve declines at t^{-1}. Due to the lack of observations between day 500 to 2500, it is not possible to predict its evolution in this time range. However, the flux seems to have increased in this gap of ∼2000 days, contrary to the expected decline. The light curve in 2–8 keV seems to have declined much faster with a power-law index of −1 throughout all the observations. In this band too, there seems to be a possible increase in the luminosity in the gap of 500–2500 days. Fortunately, *ROSAT*-PSPC observations have covered this gap with many data points in the softer band. The light curve in 0.3–2.4 keV shows an overall decline in the light curve with a power-law index of −0.25 for until about 1500 days. Thereafter, the light curve is consistent with t^{-1} decline. However, after day ∼ 200–300 the light curve reveals a sudden drop in the luminosity which rises back slowly and

---

reaches back to the -0.25 index profile by day 800. There is another possible small dip around day 1000–1500.

As discussed in Section 3, the X-rays may originate either from the forward shock or from the reverse shock. Since the density and temperature conditions of the two shocks are widely different, this information can help us identify the X-ray emission regions in a given energy band. The CS temperature can be written as

$$T_{CS} = 1.36 \times 10^9 \left(\frac{n-3}{n-2}\right)^2 \left(\frac{V_{ej}}{10^4\,\mathrm{km\,s^{-1}}}\right)^2 \mathrm{K}.$$

Radio VLBI of SN 1993J suggests an expansion velocity of the order of 7000–8000 km s^{-1} at current epoch (Bartel et al. 2007; Bartel et al. 2002). Hα observations suggest that the ejecta velocity has to be at least 7500 km s^{-1}. Fransson et al. (1996) have argued that the value of density power-law index n is 8–12. Putting these values in the above equation implies that CS temperature should be at least $T_{CS} \geqslant 50$ keV. At such a high temperature of the CS shock, there will be very little emission which will come out in the 0.3–8 keV band. At early epochs the velocities would be much higher resulting in high T_{CS}, of the order of at least few tens of keV and thus will have little flux in the energies below 8 keV. Fransson et al. (1996) have also indicated that all the flux below 10 keV is mostly arising from the reverse shock on the basis of early X-ray observations of the SN. The above discussion indicates that the 0.3–2.4 keV and 2–8 keV bands are at much lower temperatures to account for the emission from the forward shock; and most probably the X-rays in these bands are arising mostly from the reverse shock. Our claim is further strengthened by the hydrodynamic simulation (see Section 6), which also seems to suggest the reverse shock origin.

X-ray light curve behavior can give information about the nature of the reverse shock from which majority of X-rays is coming. The adiabatic shock luminosity declines with a power-law index of -1, whereas the radiative reverse shock declines much slowly. The slow decline of 0.3–8 keV light curve at early epoch is consistent with the radiative nature of the reverse shock at these epochs. The late-time -1 decline is consistent with an adiabatic reverse shock. Due to the lack of data it is not possible to pin point the transition from radiative shock to adiabatic shock. However, the soft band light curve without this gap of 2000 days clearly indicates that the shock made the transition from a radiative reverse shock to an adiabatic on around day 1500–2000. Initially hard band emission is much higher than the soft band emission but the latter dominates from day 200 onward. Since SN 1993J emission is becoming softer with time, this kind of luminosity evolution is expected. The fast decline of luminosity in 2–8 keV band also indicates that very little of this radiation is being absorbed by the cool shell in this band and most of it is coming out as adiabatic shock. The overall light curve evolution is consistent with an early radiative reverse shock turning into an adiabatic shock after around 1000 days. This kind of behavior has been predicted by Nymark et al. (2006) for such SNe. The sudden decline and gradual rise of the X-ray flux between day 200–800 and a possible dip around day 1200–1500 may be due to the density fluctuations in the ejecta. Suzuki & Nomoto (1995) had predicted a possibility of a jump in the SN 1993J light curve. They claim that while moving backward into the ejecta, the reverse shock encounters a density jump at the interface of the hydrogen envelope and the helium core. This density jump at the interface of the two regions will show up as luminosity jump in the light curve. Mioduszewski et al. (2001) clearly show the effect of this density jump on the radio emission. Suzuki &

Nomoto (1995) have calculated the possible time for this jump to be around 500–1000 days, although Mioduszewski et al. (2001) found it to be slightly later. It is probable that we are seeing this effect in the light curves of SN 1993J. However, the Suzuki & Nomoto (1995) model is one-dimensional and the strong density gradients are likely to be smoothed by instabilities.

We use the cooling time expression in Equation (2) to derive a timescale for which a reverse shock may remain radiative for the relevant parameters for SN 1993J mentioned in previous sections. A rapid cooling of the gas ahead of the shock is required such that at any stage the cooling timescale is less than the elapsed timescale so that a layer of cool and dense absorbing gas forms, i.e., $t_{cool}/t < 1$. This condition along with Equation (2) gives

$$t \leqslant \frac{(n-3)(n-4)(n-2)^{3.34}}{605} \left(\frac{\dot{M}_{-5}}{u_{w1}}\right)$$
$$\times \left(\frac{V_{ej}}{10^4\,\mathrm{km\,s^{-1}}}\right)^{-5.34} \mathrm{days}. \tag{4}$$

For $n = 12$, this equation gives $t \leqslant 260(M_{-5}/u_{w1})(V_{ej}/10^4\,\mathrm{km\,s^{-1}})^{-5.34}$ days. We tabulate radiative timescales for various values of V_{ej} and $\dot{M}_{-5}$ in Table 3. This indicates that it is possible for reverse shock to remain radiative at late epochs, as indicated by our light curves.

6. HYDRODYNAMIC SIMULATION AND COMPUTED X-RAY LIGHT CURVES

The analytic calculations in this paper assume a CS density profile that varies as r^{-2}. However, in numerical simulations, we do not constrain ourselves with r^{-2} and explore a larger parameter space. We have carried out several analytic simulations to find the best possible CSM density structure that provides an adequate fit to the observed X-ray data. We chose to reproduce the data in the hard X-ray band, because this band is likely to behave adiabatically (as evident from our 2–8 keV light curve) and hence have no complicated line emission due to the cooling effects. Our simulations are based on Mioduszewski et al. (2001) for a spherically symmetric system using high-resolution VH-1 three-dimensional finite difference code. Mioduszewski et al. (2001) produced simulated radio light curves using a detailed radiative transfer calculation and fit the radio light curve of SN 1993J. These hydrodynamic results were updated in Bartel et al. (2007) to match updated VLBI data from 1993J. Herein, we use an updated version of this hydrodynamic calculation to simulate the observed X-ray light curves of SN 1993J reported in this paper. The code computes the interaction of the ejecta with a CSM whose density profile leads to the calculation of X-ray flux density of the SN at each epoch. The calculations were carried out in one-dimensional Lagrangian coordinates and remapped on to an Eulerian grid. The shocked interaction region between the forward and reverse shocks was adequately resolved, which is important, as most of the X-rays are emitted in this region.

The hydrodynamic runs use the 4H47 ejecta density distribution model of Shigeyama and Nomoto (courtesy of K. Nomoto 1999, private communication). This model had an ejecta mass of 3.12 $M_\odot$, the pre-SN progenitor star radius of 350 $R_\odot$, and an envelope mass of 0.47 $M_\odot$. The mass fraction of helium in the envelope was about 0.79. The explosion kinetic energy was 10^{51} erg. The surrounding density profile has a slope that varies over time, from $r^{-1.4}$ in the very early stages, to $r^{-2.1}$ up to 10^{17} cm,
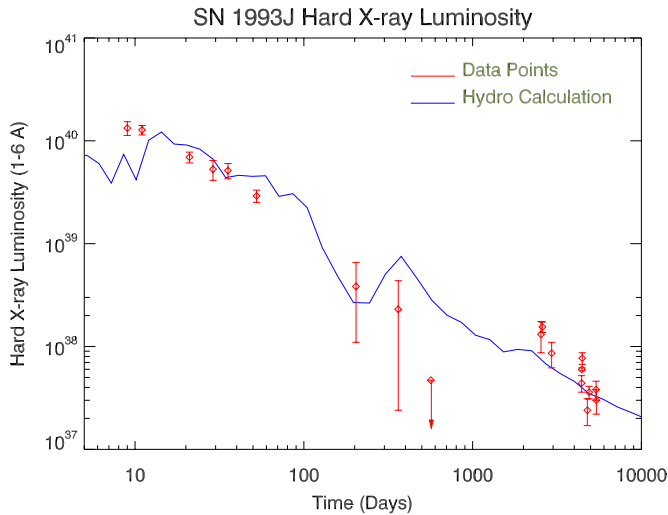
Figure 3. Model plot of the hard X-ray band (1–6 Å) luminosity evolution calculated from hydrodynamic modeling with VH-1 and CHIANTI codes starting from a Nomoto and Shigeyama 4H47 model. We plot this model with the hard band observed luminosities in 2–8 keV band. The model does not trace the early luminosity evolution for first 10–15 days (probably due to complicated X-ray emission process at early phase), however seems to reproduce the observed light curve well after that.

(A color version of this figure is available in the online journal.)

and then a steeper drop to $r^{-2.6}$ at late epochs. This CSM density profile was used to adequately fit the VLBI data in Bartel et al. (2007), and produced radii and velocities comparable to the radio and optical (Hα) observations. The computation of radiative emission from the hydrodynamic model further requires the electron temperature, whereas the hydrodynamics gives the post shock temperature, which is the temperature of the ions T_{ion}. We have found that an electron temperature about 15% of the ion temperature provides an adequate fit to the emission. This is a somewhat simplistic assumption. We calculated the X-ray emission between 1–6 Å (2–10 keV). The observational analysis show that the absorption by the cool shell is less significant for the hard X-ray emission, thus we ignore it. Line emission may also be ignored in this hard band. We used abundances that are appropriate for the ambient medium and SN ejecta in SN 1987A, as outlined by Lundqvist (1999). Nymark et al. (2009) also found the SN 1987A abundances to be a reasonable set of abundances for the SN 1993J. The ionization of various species was computed by a model due to Shull & van Steenberg (1982). Differences between various ionization models are small and do not alter the hard X-ray flux significantly, or the fundamental result that the X-ray flux arises from reverse shocked ejecta.

Given the density and temperature in every zone, the hydrodynamic model calculates the free–free and bound-free luminosity from that zone using the CHIANTI code (Dere et al. 1997). This is being done for 10,000 zones, over each time step. The contribution from each zone is added up to give the total luminosity. Having the contribution from each zone also allows us to determine exactly the part of the density profile that is contributing most to the X-ray emission. The computed X-ray luminosity in the hard band is shown in Figure 3. Looking at the simplicity of our run, the match between the simulated light curve and actual luminosity is encouraging. Between 10 and about 400 days the luminosity decreases only slowly. Some of the later peaks are due to the reverse shock running into ejecta structures which compresses them. After 1000 days, the slope becomes steeper ($L \propto t^{-1}$), in accordance with the data. We find that the hard
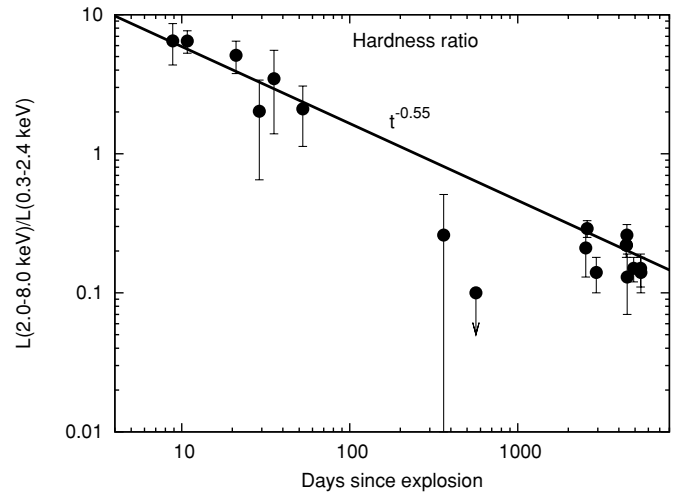
Figure 4. Here we plot the ratio of 2–8 keV luminosities vs. 0.3–2.4 keV luminosities at various epochs. The hardness ratio decreases with time and roughly follows a power-law dependence with a time index of −0.55.

X-rays arise from just behind the reverse shock. The region of hard X-ray production expands inward in the ejecta over the next decade or so till they begin to arise from most of the shocked ejecta, between the reverse shock and the contact discontinuity. After about 50 years, the forward shock starts to dominate the emission. This confirms our prediction that almost all the X-rays below 8 keV over the observed time period are coming from the reverse shock.

Our hydrodynamic simulation models are carried out in spherical symmetry. It is encouraging that even using these simple hydrodynamic models it is possible to qualitatively understand the evolution of the SN, and explore several basic features, such as the fact that the hard X-ray emission is coming predominantly from the reverse shock.

7. DISCUSSION

7.1. Column Depth and the Cool Shell

Immler et al. (2001) had analyzed *ROSAT* data fixing the column depth to be 4×10^{20} cm^{-2}, same as the Galactic absorption column density. However, the reanalysis of the same data by Zimmermann & Aschenbach (2003) and letting column density to be a free parameter revealed that column densities are much higher than the Galactic column density. Uno et al. (2002) fitted the *ASCA* data with the two-component thermal-plasma model and found that the low-temperature component has much higher column density than the high-temperature component. These high column densities in excess to the Galactic absorption can be attributed to the absorption by an additional cool shell. Since most of the X-ray emission below 8 keV is coming from the reverse shock, this indicates that both the *ROSAT* and the *ASCA* data have revealed the presence of a cool shell between the forward and a reverse shock, thus presence of a radiative reverse shock. However, the column density seems to reduce with time and after around 2000 days, the best-fit column densities are consistent with that of the Galactic absorption. This indicates that the reverse shock has most likely become adiabatic by this epoch.

7.2. Hardness Ratio and Electron Temperature

In Figure 4, we plot the ratio of SN 1993J luminosity in the 2–8 keV versus 0.3–2.4 keV bands. The figure clearly shows that

the hard X-ray emission dominates for first $\sim$100–200 days. After $\sim$200 days, soft X-ray emission starts to take over and continues to dominate. At current epoch, i.e., 15 years after the explosion, the soft X-ray is dominant by around an order of magnitude.

Since most of the flux below 8 keV is coming from the reverse shock, the ratio of the reverse shock free–free luminosity in 2–8 keV band to 0.3–2.4 keV band can be written as (Fransson et al. 1996):

$$\mathcal{H} \equiv \frac{L_{2.0-8.0~keV}}{L_{0.3-2.4~keV}} = \frac{\int_{2.0~keV}^{8.0~keV}(\frac{E}{kT})^{-0.4}\exp\left(-\frac{E}{kT}\right)\mathrm{d}E}{\int_{0.3~keV}^{2.4~keV}(\frac{E}{kT})^{-0.4}\exp\left(-\frac{E}{kT}\right)\mathrm{d}E}. \quad (5)$$

Here $(E/kT)^{-0.4}$ is the Gaunt factor in the given energy regime. This equation puts some very interesting constraint on the temperature of the reverse shock. The current hardness ratio of 0.14 corresponds to the electron temperature of 1.05 keV. This equation also shows that electron temperature was $\sim$1.5 keV around day 500 and it has evolved very slowly since then to reach the current value of 1 keV. Since free–free emission dominates above temperature 2 keV (Fransson et al. 1996), our derived temperature of 1 keV at current epoch will contribute mostly to the free–free continuum emission, as well as possibly to the line emission.

For maximum electron temperature of $\sim$30 keV (Fransson et al. 1996), the hardness ratio is 1.45. In fact, Equation (5) above reaches asymptotic upper limit of $\sim$ 1.5 which is around day 100, irrespective of temperature. However, this demonstrates that in the initial X-ray observations, where hardness ratio is larger than 1.5, the contribution between 2–8 keV is not solely because of the reverse shock but may have some contribution from the CS shock too. After day $\sim$100, all the X-ray flux below 8 keV comes from the reverse shock (see Figure 4).

7.3. Hα and the X-ray Luminosity Evolution

Hα emission in SNe arises initially by radioactivity and later by reprocessing of X-rays produced due to ejecta-wind interaction. In the case of adiabatic shocks, the Hα emission may come from the unshocked material heated by the X-rays coming from the adiabatic shock waves. If the reverse shock is radiative, then the dense cool shell between the reverse and the forward shocks may also give rise to significant Hα emission.

There have been extensive Hα observations of SN 1993J. Matheson et al. (2000a, 2000b) describe the detailed optical spectra of SN 1993J up to 2500 days. In Matheson et al. (2000b), they also measure the line widths of boxy Hα profile, an indication of the CS interaction, from day 433 onward. Patat et al. (1995) report Hα fluxes between day 171 to day 367. Zhang et al. (2004) report photometric observations of SN 1993J from the year 1995 to 2003. Houck & Fransson (1996) showed that the decay of ^{56}Ni provides the ultimate power source for Hα emission up to 250 days. After 250 days, continued presence of strong broad lines of Hα in SN 1993J have been explained as a result of photoionization by X-rays and UV emission from the radiative reverse shock propagating into the SN ejecta (Fransson et al. 2005). Patat et al. (1995) show that late-time Hα emission from SN 1993J can be described by a shell of hydrogen between 7500 and 11,400 km s^{-1}. Similar velocity range for emitting gas shells for broad, box-shaped UV lines are seen in the *HST* spectra of SN 1993J (Fransson et al. 2005) apparently coming from an ejecta and a cool dense shell.

We tabulate these Hα luminosities after day 170 in Table 4. We also plot the Hα luminosities with soft and hard band X-ray lu-

Table 4
Hα Luminosities for SN 1993J

Days Since Explosion	Luminosity (erg s^{-1})	Observatory	Reference
171	14.98×10^{38}	Asiago	Patat et al. (1995)
205	8.67×10^{38}	Asiago	Patat et al. (1995)
236	4.96×10^{38}	Asiago	Patat et al. (1995)
255	4.11×10^{38}	Asiago	Patat et al. (1995)
299	2.29×10^{38}	Asiago	Patat et al. (1995)
367	1.28×10^{38}	Asiago	Patat et al. (1995)
553	2.50×10^{38}	Lick	Matheson et al. (2000b)
670	3.00×10^{38}	Keck	Matheson et al. (2000b)
687	2.88×10^{38}	NAOC	Zhang et al. (2004)
700	2.75×10^{38}	NAOC	Zhang et al. (2004)
881	2.50×10^{38}	Lick	Matheson et al. (2000b)
976	4.80×10^{38}	Keck	Matheson et al. (2000a)
986	2.19×10^{38}	NAOC	Zhang et al. (2004)
998	1.95×10^{38}	NAOC	Zhang et al. (2004)
1034	1.99×10^{38}	NAOC	Zhang et al. (2004)
1280	1.74×10^{38}	NAOC	Zhang et al. (2004)
1318	1.29×10^{38}	NAOC	Zhang et al. (2004)
1395	1.38×10^{38}	NAOC	Zhang et al. (2004)
1729	1.10×10^{38}	NAOC	Zhang et al. (2004)
1766	0.86×10^{38}	Keck	Matheson et al. (2000b)
2066	0.65×10^{38}	NAOC	Zhang et al. (2004)
2454	0.37×10^{38}	Keck	Matheson et al. (2000b)
3149	0.50×10^{38}	NAOC	Zhang et al. (2004)
3401	0.43×10^{38}	NAOC	Zhang et al. (2004)
3503	0.43×10^{38}	NAOC	Zhang et al. (2004)
3610	0.28×10^{38}	Keck	Filippenko & Matheson (2005)
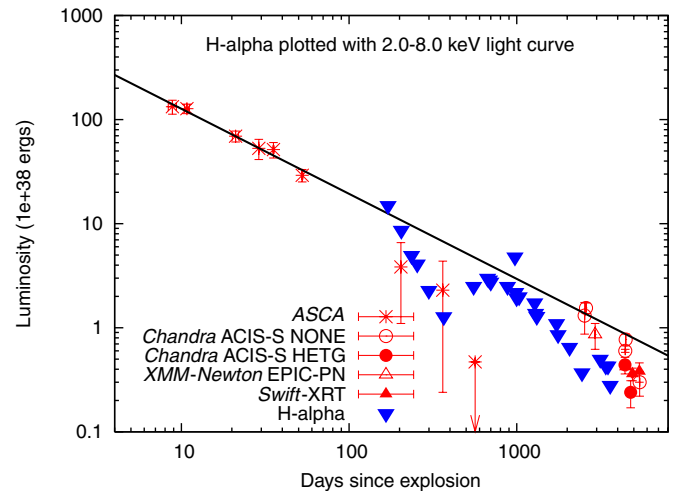
Figure 5. Plot of Hα luminosity light curve (taken from Table 4). We also plot the 2–8 keV X-ray light curve. The Hα roughly traces the 2–8 keV band light curve after day $\sim$300 indicating that Hα arises due to the CS interaction. The Hα luminosities are high fractions (30%–50%) of X-ray luminosities, which probably indicate toward the presence of clumps in the ejecta.

(A color version of this figure is available in the online journal.)

minosities in Figure 5. The figure shows that the Hα luminosity seems to follow the hard X-ray band luminosity evolution after a few hundred days, but with significant efficiency. However, it fails to trace the soft band X-rays completely. The significant rate of conversion of the kinetic luminosity of the ejecta wind interaction into broad Hα emission by the reprocessing of the X-ray luminosity of the reverse shock wave was also noted by Patat et al. (1995). It should be noted that Patat et al. (1995) have cautioned that possibly up to 30% of the emission at Hα wavelengths in SN 1993J may originate from an unidentified

band of emission around 6600 Å which is hypothesized due to a broad blend of emission lines extending between 6050 and 6800 Å as seen to be present in type Ib/Ic SNe.

The Hα seems to trace the hard band evolution but the efficiencies are 30%–50% of the X-ray production in this band, whereas the expected efficiency is typically no more than 1%–5% of the X-ray luminosity. This indicates that there could be another component which is contributing significantly to Hα flux. The clumps in the ejecta can be one such candidate which can give rise to Hα with high efficiency. The non-smooth Hα evolution also probably indicates toward the possibility of significant Hα origin from the clumps. Patat et al. (1995) also invoked an earlier suggestion by Chugai (1993) where the clumpiness of the wind material and possibly the clumpy structure of the dense and Rayleigh–Taylor unstable region in the ejecta helped attain a more efficient transformation of kinetic energy into radiation. Chugai & Danziger (1994) proposed a model for SN 1988Z, in which a radiative shock wave is driven into the dense cloud by thermal and dynamical pressures behind the main (blast wave shock and reverse shock) shock waves or by the dynamical pressures of the expanding unshocked ejecta. The shock in the cloud is significantly slower due to the higher density in the cloud and the shocked gas cools by soft X-ray or UV emission which then pumps the optical emission from the cool dense material behind the radiative shock wave in the cloud.

8. CONCLUSIONS

In this paper, we have presented the complete X-ray light curves of SN 1993J in 0.3–2.4 keV, 2–8 keV, and 0.3–8 keV bands. We demonstrate that most of the emission below 8 keV comes from the reverse shock, except for the very early soft band emission when the cool shell absorbed all the soft flux from the reverse shock. The light curves reveal that the reverse shock is radiative for around initial 1000 days and then it becomes adiabatic at later epochs, as expected for such SNe (Nymark et al. 2006). The evolution of column density too seems to indicate this. The column density was higher than the Galactic column density during the *ROSAT*, *ASCA,* and early *Chandra* and *XMM-Newton* observations, and later became comparable to the Galactic absorption, indicating the presence of a cool shell during the first 1000 days. We demonstrate that for SN 1993J parameters, it is possible for the shock to be radiative at such late epochs.

We have carried out numerical hydrodynamic computations, and calculated the hard X-ray flux from the same, which agree reasonably well with the observed data. Our simulations clearly show that all the emission below 8 keV is indeed coming from the reverse shock, strengthening our claim.

The large fraction of Hα flux in comparison to the X-ray emission indicates possibility of clumps in the ejecta.

One of the important questions is how these young SNe evolve toward a SNR. Since young SNe and older SNRs are both products of explosive events a natural question is whether the former evolve continuously into the latter with time, whether similar emission mechanisms differing only in length-scales and timescales operate or if the SNe fade away only to switch on later as SNRs with a different mechanism of radiation. One of the very well studied SNR in our galaxy, Cassiopeia A was thought to be of the Type IIb or IIn (Chevalier & Oishi 2003). However, it has recently been conclusively classified as a Type IIb SN, the same type as that of SN 1993J (Krause et al. 2008). Late-time observations of SN 1993J may provide an important link between young SNe and SNRs. SN 1993J had a large X-ray

flux, which, coupled with it being a nearby SN, made it easily observable for a long time with a well sampled light curve. This has made SN 1993J one of the best studied extragalactic SNe, and provided a wealth of information on SN evolution and their CS interaction. Further observations of this SN for a long time is sure to provide much valuable information on these questions.

REFERENCES

Bartel, N., Bietenholz, M. F., Rupen, M. P., & Dwarkadas, V. V. 2007, ApJ, 668, 924
Bartel, N., et al. 2002, ApJ, 581, 404
Burrows, D. N., et al. 2005, Space Sci. Rev., 120, 165
Chandra, P., Ray, A., Schlegel, E. M., Sutaria, F. K., & Pietsch, W. 2005, ApJ, 629, 933
Chevalier, R. A., & Fransson, C. 1994, ApJ, 420, 268
Chevalier, R., & Fransson, C. 2003, in Lecture Notes in Physics 598, Supernovae and Gamma-Ray Bursters, ed. K. Weiler (Berlin: Springer-Verlag), 171
Chevalier, R., & Oishi, J. 2003, ApJ, 593, L23
Chevalier, R., & Soker, N. 1989, ApJ, 341, 867
Chugai, N. 1993, ApJ, 414, L101
Chugai, N., & Danziger, J. 1994, MNRAS, 268, 173
Dere, K. P., Landi, E., Mason, H. E., Monsignori Fossi, B. C., & Young, P. R. 1997, A&AS, 125, 149
Filippenko, A. V., & Matheson, T. 2005, in IAU Coll. 192, Cosmic Explosions, On the 10th Anniversary of SN1993J, ed. J. M. Marcaide & K. W. Weiler (Berlin: Springer), 37
Filippenko, A. V., Matheson, T., & Woosley, S. E. 1993, IAU Circ., 5787, 1
Fransson, C., & Bjornsson, C. I. 1998, ApJ, 509, 861
Fransson, C., Lundqvist, P., & Chevalier, R. A. 1996, ApJ, 461, 993
Fransson, C., & Sonneborn, G. 1994, in Frontiers of Space and Ground Based Astronomy, Astrophysics an Space Science Library 187, ed. W. Wamsteker et al., 249
Fransson, C., et al. 2005, ApJ, 622, 991
Freedman, W. L., et al. 1994, ApJ, 427, 628
Gehrels, N., et al. 2004, ApJ, 611, 1005
Gröningsson, P., Fransson, C., Lundqvist, P., Nymark, T., Lundqvist, N., Chevalier, R., Leibundgut, B., & Spyromilio, J. 2006, A&A, 456, 581
Houck, J. C., & Fransson, C. 1996, ApJ, 456, 811
Immler, S., Aschenbach, B., & Wang, Q. D. 2001, ApJ, 56, L107
Kohmura, Y., et al. 1994, PASJ, 46, L157
Krause, O., Birkmann, S. M., Usuda, T., Hattori, T., Goto, M., Rieke, G. H., & Misselt, K. A. 2008, Science, 320, 1195

Leising, M. D., et al. 1994, ApJ, 431, L95
Lundqvist, P. 1999, ApJ, 511, 389
Matheson, T., et al. 2000, AJ, 120, 1487
Matheson, T., et al. 2000, AJ, 120, 1499
Matzner, C. D., & McKee, C. F. 1999, ApJ, 510, 379
Maund, J., et al. 2004, Nature, 427, 129
Mioduszewski, A. J., Dwarkadas, V. V., & Ball, L. 2001, ApJ, 562, 869
Nomoto, K., & Suzuki, T. 1998, The Hot Universe, 188, 27
Nomoto, K., et al. 1993, Nature, 364, 507
Nymark, T. K., Chandra, P., & Fransson, C. 2009, A&A, 494, 179
Nymark, T. K., Fransson, C., & Kozma, C. 2006, A&A, 449, 171
Patat, F., Chugai, N., & Mazzali, P. A. 1995, Astron. Astrophys., 299, 715
Podsiadlowski, P., Hsu, J. J. L., Joss, P. C., & Ross, R. R. 1993, Nature, 364, 509
Ray, A., Singh, K. P., & Sutaria, F. K. 1993, J. Astrophys. Astron., 14, 53
Ripero, J., & Garcia, F. 1993, IAU Circ., 5731, 1

Shull, J. M., & van Steenberg, M. 1982, ApJS, 48, 95
Suzuki, T., Kumagai, S., Shigeyama, T., Nomoto, K., Yamaoka, H., & Saio, H. 1993, ApJ, 419, L73
Suzuki, T., & Nomoto, K. 1995, ApJ, 455, 658
Swartz, D. A., et al. 2003, ApJS, 144, 213
Tanaka, Y. 1993, IAU Circ., 5753, 1
Truelove, J. K., & McKee, C. F. 1999, ApJS, 120, 299
Uno, S., et al. 2002, ApJ, 565, 419
Van Dyk, S. D., et al. 1994, ApJ, 432, L115
Woosley, S. E., Eastman, R. G., Weaver, T. A., & Pinto, P. A. 1994, ApJ, 429, 300
Zhang, T., Wang, X., Zhou, X., Li, W., Ma, J., Jiang, Z., & Li, Z. 2004, AJ, 128, 1857
Zimmermann, H.-U., & Aschenbach, B. 2003, A&A, 406, 969
Zimmermann, H. U., et al. 1993, IAU Circ., 5748, 1
Zimmermann, H.-U., et al. 1994, Nature, 367, 621